Dynamic Light Scattering from a Nematic Monodomain Containing a Side-Chain Liquid Crystal Polymer in a Nematic Solvent

Dongfeng Gu, Alex M. Jamieson,* Charles Rosenblatt, Dimitri Tomazos, Myongsoo Lee, and Virgil Percec

Departments of Macromolecular Science and Physics, Case Western Reserve University, Cleveland, Ohio 44106

Received July 11, 1990; Revised Manuscript Received November 14, 1990

ABSTRACT: By combining dynamic light scattering data on nematic monodomains in three different scattering configurations with independent measurements on the bend elastic constant via the Freedericksz transition method, we have measured all of the elastic and viscosity coefficients associated with the splay, bend, and twist distortions of the nematic matrix. We performed VH scattering experiments on monodomains in the homogeneous orientation, with the nematic director aligned, respectively, inside and orthogonal to the plane formed by the incident and scattered wave vectors. Similar studies were carried out on homeotropic monodomains with the nematic director parallel to the incident wave vector. Numerical values of elastic and viscosity constants derived from such analyses on pure pentacyanobiphenyl (5CB) are consistent with literature results. The addition of a side-chain liquid crystal polymer, poly[6-(4-methoxy-α-methylstilben-4′-yl)oxy]hexyl methacrylate] (MSHMA), results in significant increases in the relaxation times for dynamic light scattering from all three scattering geometries. These changes are due to small decreases of the three elastic constants and larger increases of the three viscosities. Increase of polymer molecular weight results in a relatively small change in the elastic constants and a substantial increase in all three viscosities. The percent change is largest for the bend mode and smallest for the splay mode, which is consistent with the idea that the former involves translational motions of the backbone, whereas the latter requires relatively unhindered rotations around the backbone.

Introduction

The theoretical and experimental basis for applying the dynamic light scattering experiment to obtain information on the viscoelastic constants of the nematic liquid crystal materials is well established.[1-6] Light is scattered by long-wavelength fluctuations of the nematic director $\hat{\mathbf{n}}_o$, which results in two diffusive deformation modes corresponding to splay–bend and twist–bend distortions of the nematic matrix. The differential scattering cross section per unit volume is given by[1-6]

$$\frac{d\sigma}{d\Omega} = \left(\frac{\pi\epsilon_a}{\lambda^2}\right)^2 k_B T \sum_{\nu=1,2} \frac{(i_\nu f_z + i_z f_\nu)}{K_{33} q_\parallel^2 + K_{\nu\nu} q_\perp^2} \tag{1}$$

The scattering vector $\vec{q} = \vec{k}_i - \vec{k}_f$, where $\vec{k}_i$ and $\vec{k}_f$ refer to the incident and scattered wave vectors, and $\hat{i}$ and $\hat{f}$ are unit vectors defining the incident and scattered polarizations. Equation 1 is based on a Cartesian coordinate system (x, y, z) with the z axis defining the optic axis ($\hat{\mathbf{n}}_o$) of the nematic and with two unit vectors $\hat{e}_1$ and $\hat{e}_2$ oriented in the x, y plane such that

$$\hat{e}_1 = \frac{\hat{e}_2 \times \hat{z}}{|\hat{e}_2 \times \hat{z}|}$$

and

$$\hat{e}_2 = \frac{\hat{z} \times \hat{q}}{|\hat{z} \times \hat{q}|}$$

The components of $\hat{i}$ and $\hat{f}$ along $\hat{e}_\nu$ are called i_ν and f_ν and those along the z axis, i_z and f_z. In a similar fashion, the component of $\vec{q}$ parallel to the director is $q_\parallel = q_z$, and the component of $\vec{q}$ orthogonal to $\hat{\mathbf{n}}_o$ is $q_\perp$. $\epsilon_a = \epsilon_\parallel - \epsilon_\perp$ is the anistropy of the dielectric constant, λ the wavelength of light, k_B Boltzmann's constant, and T the absolute temperature. K_{33} refers to the bend elastic constant, and $K_{\nu\nu}$, $\nu = 1, 2$, are the splay and twist elastic constants. Note that in the following analysis we use two other scattering configurations in which $\hat{\mathbf{n}}_o$ is oriented, respectively, along the x and y axes. For these situations, equations equivalent to those above for $d\sigma/d\Omega$ and $\hat{e}_1$ and $\hat{e}_2$ are obtained but with z replaced everywhere by x and y, respectively.

The mean relaxation frequencies of the two director deformation modes can be determined by photon correlation analysis of the scattered light[1-6] and are given by

$$\Gamma_\nu(q) = \frac{(K_{33} q_\parallel^2 + K_{\nu\nu} q_\perp^2)}{\eta_\nu(q)} \tag{2}$$

where $\eta_\nu(q)$ are two viscosity functions:

$$\eta_1(q) = \gamma_1 - \frac{(q_\perp^2 \alpha_3 - q_\parallel^2 \alpha_2)^2}{q_\perp^4 \eta_b + q_\perp^2 q_\parallel^2 (\alpha_1 + \alpha_3 + \alpha_4 + \alpha_5) + q_\parallel^4 \eta_c} \tag{3}$$

$$\eta_2(q) = \gamma_1 - \frac{\alpha_2^2 q_\parallel^2}{q_\perp^2 \eta_a + q_\parallel^2 \eta_c} \tag{4}$$

In eqs 3 and 4, the α_i refer to the five Leslie viscosity coefficients,[7] γ_1 is the twist viscosity,[1] and η_a, η_b, and η_c are the Miesowicz viscosities.[8]

In our experiments, we have utilized the three scattering configurations shown in Figure 1. Configuration A utilizes a homogeneously aligned monodomain with the director perpendicular to the scattering plane formed by $\vec{k}_i$ and $\vec{k}_f$, and with $\hat{i} \parallel \hat{z}$ and $\hat{f} \perp \hat{z}$. Here $q_\parallel = 0$ and $q_\perp = (2\pi/\lambda)[n_o^2 \sin^2\theta_o + (n_e - n_o \cos\theta_o)^2]^{1/2}$, where n_o and n_e are the temperature-dependent ordinary and extraordinary refractive indices of the nematic and θ_o is the scattering angle inside the nematic sample. From eqs 2–4, it follows that scattering modes 1 and 2 become, respectively, pure splay and pure twist. Thus, light scattering measurements detect the sum of each mode, weighted by the geometric

0024-9297/91/2224-2385$02.50/0

factors, $(i_1f_z + i_zf_1)^2 = n_e^2 \sin^2\theta/[n_o^2 \sin^2\theta + (n_e - n_o \cos\theta)^2]$, and $(i_2f_z + i_zf_2)^2 = (n_o - n_e \cos\theta)^2/[n_o^2 \sin^2\theta + (n_e - n_o \cos\theta)^2]$. Thus

$$\frac{d\sigma}{d\Omega} = \left(\frac{d\sigma}{d\Omega_1}\right) + \left(\frac{d\sigma}{d\Omega_2}\right) \tag{5}$$

where

$$\left(\frac{d\sigma}{d\Omega_1}\right) = \left(\frac{\epsilon_a}{2\lambda}\right)^2 k_B T \left\{\frac{n_e^2 \sin^2\theta_o}{K_{11}[(n_e - n_o\cos\theta_o)^2 + n_o^2\sin^2\theta_o]^2}\right\} \tag{6}$$

and

$$\left(\frac{d\sigma}{d\Omega_2}\right) = \left(\frac{\epsilon_a}{2\lambda}\right)^2 k_B T \left\{\frac{(n_o - n_e\cos\theta)^2}{K_{22}[(n_e - n_o\cos\theta_o)^2 + n_o^2\sin^2\theta_o]^2}\right\} \tag{7}$$

The decay rates are

$$\Gamma_1 = K_{11}q_\perp^2/\left(\gamma_1 - \frac{\alpha_3^2}{\eta_b}\right) = K_{11}q_\perp^2/\eta_{splay} \tag{8}$$

and

$$\Gamma_2 = K_{22}q_\perp^2/\gamma_1 \tag{9}$$

where $\eta_{splay} = (\gamma_1 - \alpha_3^2/\eta_b)$ is the viscosity of the splay distortion. Note that when the polarization condition $(i_2f_z + i_zf_2) = 0$ is met approximately, only splay mode is sampled in the experiment.

Configuration B again uses a homogeneously aligned monodomain but has the director in the scattering plane, $\hat{n}_o \| \hat{x}$ and $\hat{n}_o \perp \vec{k}_i$, with $\hat{i} \| \hat{z}$ and $\hat{f}$ in the scattering plane. Here, the geometric factor $(i_1f_x + i_xf_1) = 0$ and hence $d\sigma/d\Omega_1 = 0$. The scattered intensity is determined by mode 2, with $(i_2f_x + i_xf_2) = \cos\theta_o$, $q_\parallel = (2\pi n_e/\lambda)\sin\theta_o$, and $q_\perp = (2\pi/\lambda)(n_e\cos\theta_o - n_o)$

$$\frac{d\sigma}{d\Omega} = \left(\frac{d\sigma}{d\Omega_2}\right) = \left(\frac{\epsilon_a}{2\lambda}\right)^2 k_B T \frac{\cos^2\theta_o}{K_{22}(n_e\cos\theta_o - n_o)^2 + K_{33}n_e^2\sin^2\theta_o} \tag{10}$$

and

$$\Gamma_2 = \frac{K_{22}q_\perp^2 + K_{33}q_\parallel^2}{\left[\gamma_1 - \dfrac{\alpha_2^2 q_\parallel^2}{\eta_a q_\perp^2 + \eta_c q_\parallel^4}\right]} \tag{11}$$

When $q_\perp = 0$ ($\theta \sim 24°$ in our experiment), $\Gamma_2 = K_{33}q_\parallel^2/\eta_{bend}$, where $\eta_{bend} = \gamma_1 - \alpha_2^2/\eta_c$.

Finally, configuration C utilizes a homeotropically aligned monodomain with the director again in the scattering plane, with $\hat{n}_o \| \hat{y}$ and $\hat{n}_o \| \vec{k}_i$. Here we have $(i_1f_y + i_yf_1) = 0$ and $(d\sigma/d\Omega_1) = 0$. Now, however, $(i_2f_y + i_yf_2) = \sin\theta_o$, $q_\parallel = (2\pi/\lambda)(n_e\cos\theta_o - n_o)$ and $q_\perp = (2\pi n_e/\lambda)\sin\theta_o$. Thus

$$\frac{d\sigma}{d\Omega} = \left(\frac{d\sigma}{d\Omega_2}\right) = \left(\frac{\epsilon_a}{2\lambda}\right)^2 k_B T \frac{\sin^2\theta_o}{K_{22}n_e^2\sin^2\theta_o + K_{33}(n_e\cos\theta_o - n_o)^2} \tag{12}$$

The decay rate is again given by eq 11. Note that the term θ_o in eqs 5–12 refers to the scattering angle inside the nematic sample, related to the scattering angle, θ, in the laboratory frame by Snell's law, viz. $n\sin\theta_o = n_T\sin\theta$.

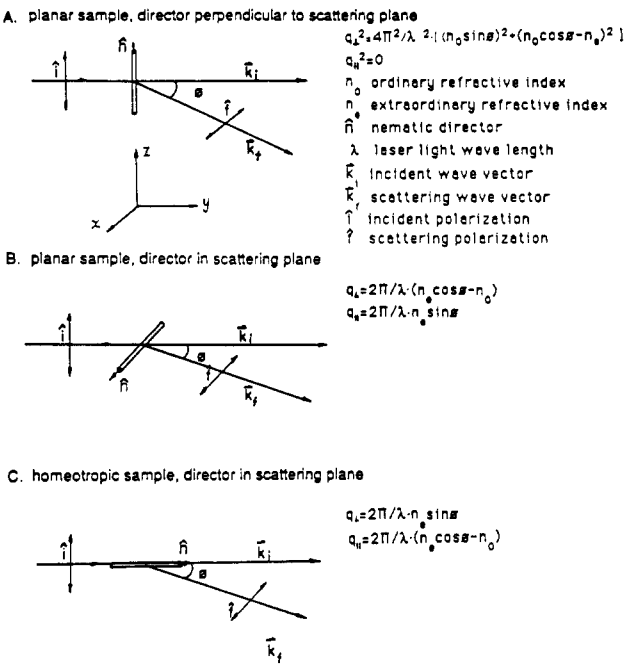

Figure 1. Three different scattering geometries used in our experiments: A selects mode 1 (pure splay) + mode 2 (pure twist); B selects mode 2 (twist–bend); C selects mode 2 (twist–bend).

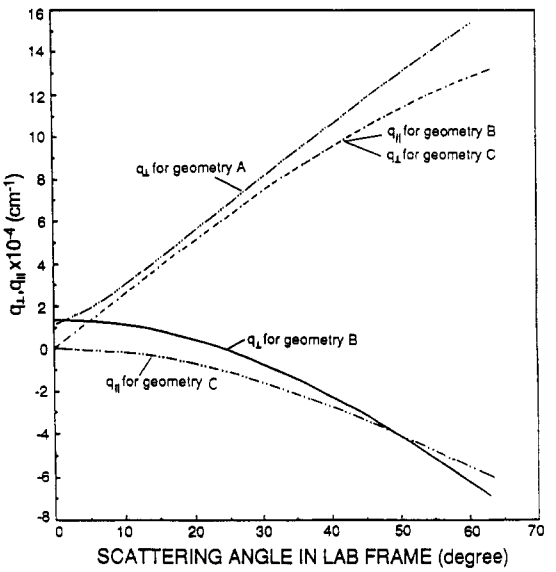

Figure 2. Numerical values of scattering vectors $q_\parallel$ and $q_\perp$ as a function of scattering angle in the laboratory frame. Note that $q_\parallel$ (– · –) in geometry B is the same as $q_\perp$ (- - -) in geometry C, while $q_\perp$ (—) in geometry B is different from $q_\parallel$ (– ·· –) in geometry C. In geometry A, only $q_\perp$ (– ··· –) $\neq 0$.

Here n_T is the refractive index of toluene, used as matching liquid, and n is the refractive index inside the sample. The configuration A, $n = n_o$, and $n_e = n_\parallel$; in configuration B, $n = n_e$ and $1/n_e^2 = \sin^2\theta_o/n_o^2 + \cos^2\theta_o/n_\parallel^2$; in configuration C, $n = n_e$ and $1/n_e^2 = \cos^2\theta_o/n_o^2 + \sin^2\theta_o/n_\parallel^2$, where $n_\parallel$ is the semimajor axis of the Fresnel index ellipsoid (maximum of n_e) of the nematic.[9] Figure 2 shows the dependence of $q_\perp$ and $q_\parallel$ on scattering angle in the three configurations. Evidently there are substantial differences in both magnitude and curvature of $q_\perp$ and $q_\parallel$ for these configurations, suggesting that by combining light scattering data over a wide range of scattering angles in all three configurations, it is possible to facilitate extraction of the numerical values of the various elastic and viscosity coefficients.

A direct approach to the determination of the elastic constants, K_{ii}, is via the Freedericksz transition method.[10] The elastic constant is computed from the critical magnetic field necessary to produce a specified director distortion in a monodomain sample. Likewise, certain of the viscosity efficients can be obtained by conventional viscometric experiments in the presence of an applied magnetic field. Since estimation of the viscoelastic properties from light scattering data via eqs 1–12 requires a multiparameter least-squares fit, it is clear that independent determination of one or more parameters assists in obtaining a unique solution. In this study, we have obtained independent measurements of K_{33} via the Freedericksz transition technique.

Early light scattering studies focused on analyses of the properties of low molar mass nematics. More recently, investigations of liquid crystal materials containing polymeric nematogens have been reported. Two types of systems have been studied. One class consists of the lyotropic liquid crystals formed by semirigid polymers.[11] A second group comprises miscible thermotropic liquid crystal mixtures composed of a low molar mass and a polymeric mesogen.[5,12] Experimental studies on the latter materials have involved reports of bend, splay, and twist elastic constants, as well as twist viscosities of mixtures of side-chain liquid crystal polymers, based on a polysiloxane backbone, in cyanobiphenyl-based species as solvents.[5] The addition of polymer results in a progressive decrease in all three elastic constants. However, the bend constant K_{33} is most influenced.[13] The twist viscosity is substantially increased as a function of polymer concentration in the mixtures.[14]

In this study we report dynamic light scattering experiments on monodomains formed from pentylcyanobiphenyl (5CB) and from miscible mixtures of 5CB with a side-chain liquid crystal polymer (LCP), poly[6-(4-methoxy-α-methylstilben-4′-yl)oxy]hexyl methacrylate] (MSHMA). By combining data on the three scattering geometries listed above, we obtain information on all three elastic and viscosity coefficients. An independent measurement of the bend elastic constant for both 5CB and several of the polymer mixtures has been obtained via the Freedericksz method.

Experimental Methods

Pentylcyanobiphenyl (5CB) was obtained from BDH Chemicals and used as received. The nematic–isotropic transition temperature is T_{NI} = 35.1 °C. The side-chain LCP utilized in our study was synthesized by Professor Virgil Percec and co-workers[15] and consists of a poly(methyl methacrylate) backbone to which the pendant mesogenic groups (4′-α-methylstilbene) are attached via a flexible hexamethylene spacer. Three polymer samples of different molecular weights were utilized in our studies: MSHMA/36, M_n = 3600; MSHMA/45, M_n = 4500, and MSHMA/570, M_n = 57 000, as determined by gel permeation chromatography in tetrahydrofuran using polystyrene standards. For all samples, $M_w/M_n \cong 1.35$. The polymer exhibits a nematic phase in the temperature range studied with a $T_{NI} = \sim 94$ °C. A smectic A phase is obtained on annealing with a T_{NA} = 18 °C. Monodomain samples, as verified by optical microscopy, were prepared between clean microscopic slides, separated by Mylar spacers with thicknesses of 12.5 and 50 μm. Specimens in the homogeneous orientation were obtained by the classical rubbing technique; specimens in the homeotropic alignment were prepared by treating the glass surfaces with a surfactant, hexadecyltrimethylammonium bromide (HTAB). For the LCP concentration range utilized for our samples, we verified using optical microscopy that the samples were miscible in both the nematic and isotropic phases, with a narrow biphasic region at the transition. The temperature extent of this region was proportional to the LCP concentration. The refractive indices of pentylcyanobiphenyl and the polymer have been determined by other groups.[16,17]

Photon correlation analysis of the light scattered from the nematic monodomains was performed by using an instrument (Brookhaven Instruments Corp., Ronkonkoma, NY) equipped with a 15-mW He/Ne laser and a BI 2030 AT 256-channel digital correlator. The sample was positioned in a refractive index-matching bath by using a custom-designed micromanipulator which enables us to make small adjustments to keep the scattering volume in the focal plane of the collecting lens at all scattering angles. The sample temperature was controlled by a refrigerated circulating bath accurate to better than 0.1 °C. In photon correlation spectroscopy we obtain the intensity autocorrelation function, normalized to the calculated baseline

$$G_2(t) = \langle n(0)n(t)\rangle / \langle n(0)n(0)\rangle$$

where $n(t)$ refers to the detected photon counts at time increment, t, and the brackets refer to a time average. $G_2(t)$ is related to the electric field correlation function, $g_1(t)$, by the relation

$$G_2(t) = 1 + f(A)|g_1(t)|^2$$

where $f(A)$ is a parameter that depends on the coherence matching of the scattered radiation at the detector. By employing the micropositioner, we are able to routinely obtain $f(A) \gtrsim 0.8$ at all scattering angles. $g_1(t)$ has the general form

$$g_1(t) = \int_0^\infty G(\Gamma)e^{-\Gamma t}\,d\Gamma$$

where $G(\Gamma)$ is the distribution of relaxation frequencies which characterize the dissipative behavior of the director fluctuations which are the source of the depolarized light scattering. We analyze $g_1(t)$ by least-squares fits to a cumulant expansion

$$\log_e g_1(t) = -\bar{\Gamma}t + \mu_2 t^2 - \ldots$$

where $\bar{\Gamma} = \int_0^\infty G(\Gamma)\Gamma\,d\Gamma$ is the mean decay rate and $\mu_2 = \int_0^\infty G(\Gamma)(\Gamma - \bar{\Gamma})^2\,d\Gamma$ is the variance of Γ. For all of the correlation data pertinent to this study, $g_1(t)$ exhibited a single-exponential decay, i.e., $\mu_2 = 0$, within experimental error.

We also performed magnetic Freedericksz transition measurements on homeotropic samples with the magnetic field perpendicular to the director. This determines K_{33}.[10] The sample thicknesses d were all in the neighborhood of 13 μm and determined interferometrically to better than 1%. The samples were housed in a temperature-controlled oven inserted into the base of an 8.2-T superconducting magnet with optical axis perpendicular to the field. The field was ramped at 8 G/s and the transmitted laser intensity computer recorded. No hysteresis was observed in the threshold field H_{th}. The order parameter vs temperature was obtained from birefringence measurements, and, in conjunction with magnetic susceptibility data from the literature,[21] we obtained $\Delta\chi$ vs T. Finally, K_{33} was extracted:

$$K_{33} = \frac{d^2 H_{th}^{\,2}}{\pi^2}\Delta\chi$$

Results and Discussion

In Figure 3a, we present Freedericksz transition results for the temperature dependence of K_{33} for pure 5CB and mixtures containing 3.2% and 5.3% w/w polymer (MSHMA/3.5). We note first that the experimental data for pure 5CB are in excellent agreement with literature values.[18] Next, we see that addition of polymer results in a decrease of K_{33} at a given temperature. This effect is clearly due to the depression in T_{NI} with polymer concentration, resulting in less orientational order at a given temperature. Thus, K_{33} was found to increase slightly with LCP concentration when plotted directly against the nematic order parameter $S = \Delta\chi/\Delta\chi_{sat}$ as shown in Figure 3b. Note that, in evaluating K_{33} for the mixtures, we have assumed that the saturated susceptibility anisotropy, $\Delta\chi_{sat}$, and the refractive indices, n_e and n_o, are the same as for pure 5CB. The latter assumption is also made in interpreting the light scattering data below. Since the differ-

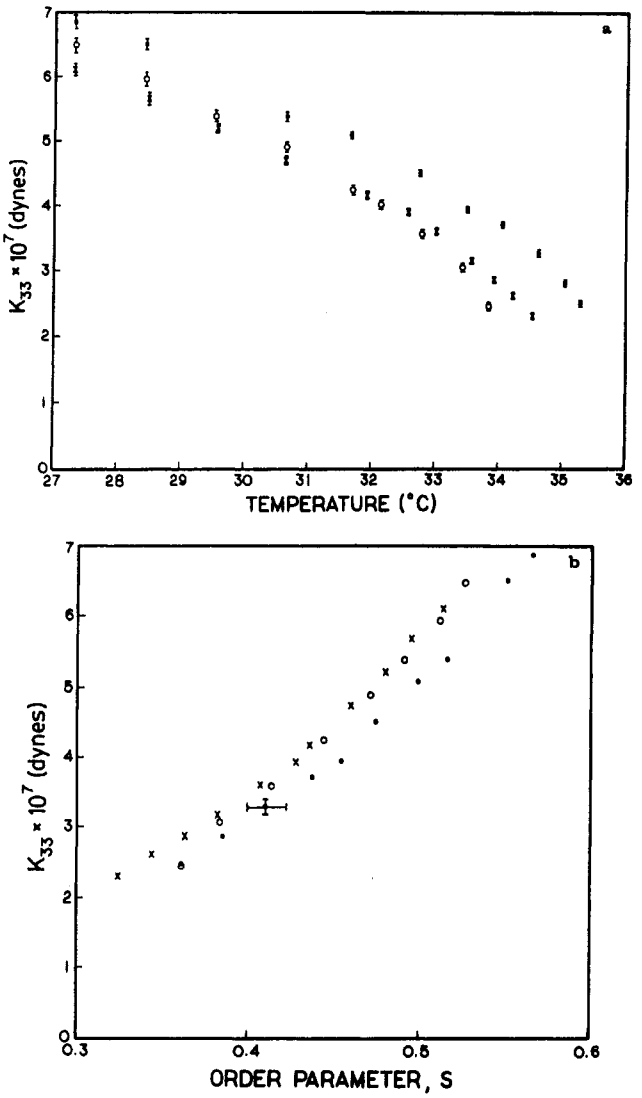

Figure 3. Measured band elastic constant K_{33} with different LCP concentrations [(●) 5CB; (○) 3.2% LCP + 5CB; (×) 5.3% LCP + 5CB] plotted against temperature (a) and against the order parameter (b).

ences between the refractive indices of pure 5CB and MSHMA are small (n_o = 1.537, n_e = 1.680 for 5CB; n_o = 1.550, n_e = 1.615 for MSHMA at T = 33 °C),[16,17] these approximations are expected to introduce negligible errors, particularly in view of the low LCP concentrations utilized in this study. This was confirmed by examining the effect of varying n_e and n_o in our data-fitting procedures.

Measured decay rates based on single-exponential fits to photon correlation spectroscopy of pure 5CB and a 3.2% w/w polymer/5CB mixture in scattering configurations A–C are compared in the angular range $10° < \theta < 60°$ in Figures 4–6. Also shown are calculated decay rates computed from fits to the experimental data based on eqs 8 and 11. The calculated values at all scattering angles are generally in good agreement with experiment, except in the case of configuration A. Here we have shown a fit of the experimental data to mode 1 alone (pure splay), since $d\sigma/d\Omega_2$:$d\sigma/d\Omega_1 < 1{:}20$ in the scattering angle range $15° < \theta < 35°$. Systematic deviations are noted in Figure 4 at larger scattering angles. This is because of the increasing contributions of mode 2 (pure twist) in this geometry at angles $\theta < 35°$. Similar deviations are expected at small angles $\theta < 15°$. In these fits, initial values of the bend elastic constant were chosen on the basis of the Freedericksz transition results. For the mixtures, several

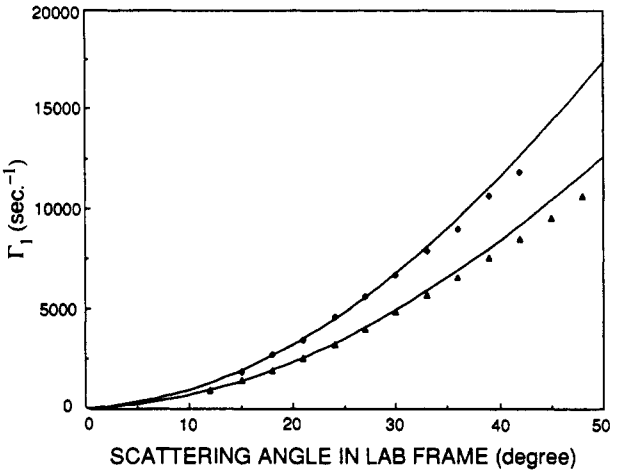

Figure 4. Experimental and calculated decay rates of dynamic light scattering from pure 5CB and the LCP mixture (M_n = 4500, C = 3% w/w) for geometry A at T = 33 °C: (—) calculated; (◆) measured for pure 5CB; (▲) measured for 3% LCP mixture. Calculated values are for mode 1 only; deviations between experiment and calculation at higher scattering angles are due to contributions from mode 2.

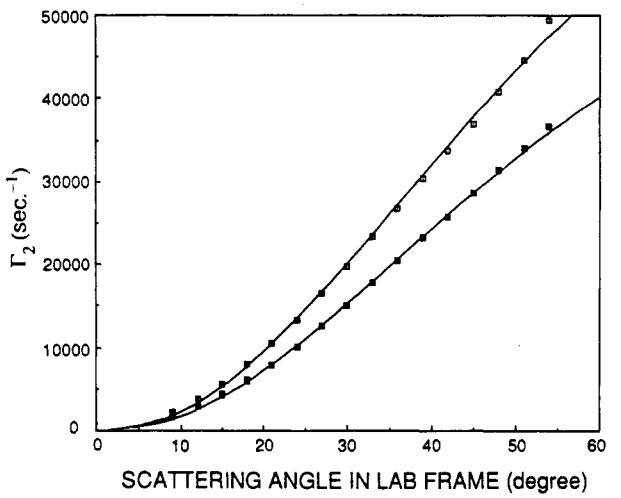

Figure 5. Experimental and calculated decay rates of dynamic light scattering from pure 5CB and the LCP mixture (M_n = 4500, C = 3% w/w) for geometry B at T = 33 °C: (—) calculated; (□) measured for pure 5CB; (■) measured for 3% LCP mixture.

constraints are invoked: the K_{ii} are numerically smaller than the values for pure 5CB and are assumed to decrease monotonically with polymer concentration; the viscosity coefficients are larger than those for pure 5CB and assumed to increase monotonically with polymer concentration. Calculated and experimental values of the decay rates in all three configurations agree to within 3% at all scattering angles. With these criteria, we are able to specify the estimated viscoelastic parameters to within limits shown in Table I. Here, we list the experimental values of the intrinsic decay rates for light scattering from the splay, twist, and bend distortions: $\tilde{\Gamma}_{splay} = K_{11}/\eta_{splay}$, $\tilde{\Gamma}_{twist} = K_{22}/\gamma_1$, and $\tilde{\Gamma}_{bend} = K_{33}/\eta_{bend}$. Also listed are the values of the individual elastic and viscosity coefficients deduced on the basis of the fits shown in Figures 4–6.

For pure 5CB, our experimental results are in good agreement with selected literature values. For example, a direct comparison of the decay rates for light scattering from the twist distortions of pure 5CB, $\tilde{\Gamma}_{twist} = K_{22}/\gamma_1$, between our results and published data of Sefton et al.[5] is shown in Figure 7. Further, viscosity values determined in our study are numerically similar to those reported for

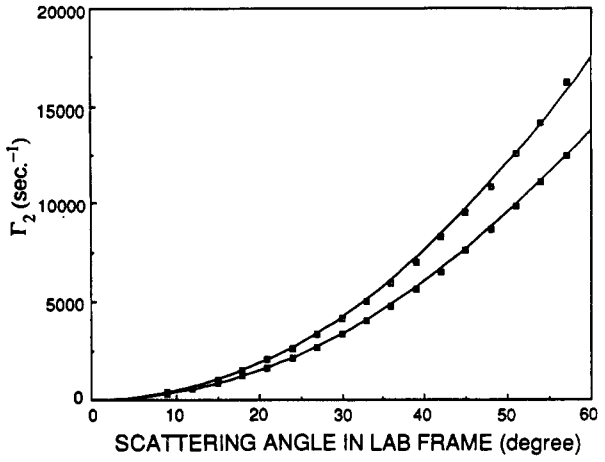

Figure 6. Experimental and calculated decay rates of dynamic light scattering from pure 5CB and the LCP mixture (M_n = 4500, C = 3% w/w) for geometry C at T = 33 °C. Symbols used here are as in Figure 5.

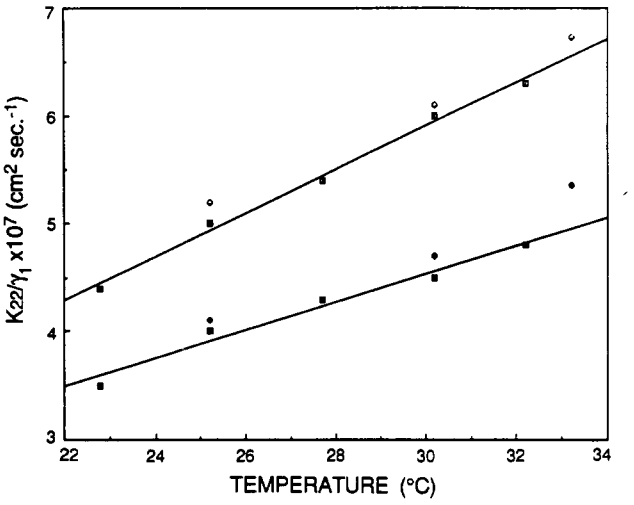

Figure 7. Comparison of measured ratio of K_{22}/γ_1 for scattering from pure twist with literature values: (Sefton et al.) ⊡ = 5CB, ■ = 5CB + 2% LCP; (this work) ◇ = 5CB, ◆ = 5CB + 3% LCP.

Table I
Temperature Dependence of Viscoelastic Parameters for 5CB and 3% w/w LCP/5CB Mixture (M_n = 4500)

	T = 25 °C		T = 30 °C		T = 33 °C	
	5CB	LCP/5CB	5CB	LCP/5CB	5CB	LCP/5CB
10^8K_{11} ± 5%, dyn	62	58	45	41	30	26
10^8K_{22} ± 3%, dyn	43	37	31	25	21	19
10^8K_{33} ± 3%, dyn	31	61	54	45	41	33
η_{splay} ± 1%, P	0.83	0.89	0.48	0.52	0.29	0.35
γ_1 ± 1%, P	0.83	0.91	0.50	0.53	0.30	0.36
η_{bend} ± 2%, P	0.14	0.18	0.12	0.18	0.11	0.12
$10^7K_{11}/\eta_{splay}$ ± 5%, cm^2/s	7.47	6.52	9.38	7.89	10.3	7.43
$10^7K_{22}/\gamma_1$ ± 3%, cm^2/s	5.18	4.01	6.10	4.72	6.83	5.36
$10^7K_{33}/\eta_{bend}$ ± 3%, cm^2/s	57.9	33.9	45.0	25.0	37.3	27.2

5CB by Skarp et al.[19] Likewise K_{11} and K_{33} values obtained by us for 5CB agree very well with results reported by several groups. Finally, K_{22} values computed from our light scattering data yield ratios K_{33}/K_{22} which are reasonably consistent with corresponding values obtained by Hara et al.[20]

Table I indicates that addition of LCP to 5CB results in a substantial decrease in all three intrinsic decay rates, $\tilde{\Gamma}_{splay}$, $\tilde{\Gamma}_{twist}$, and $\tilde{\Gamma}_{bend}$. The source of this change is a decrease in the associated elastic constant and an increase

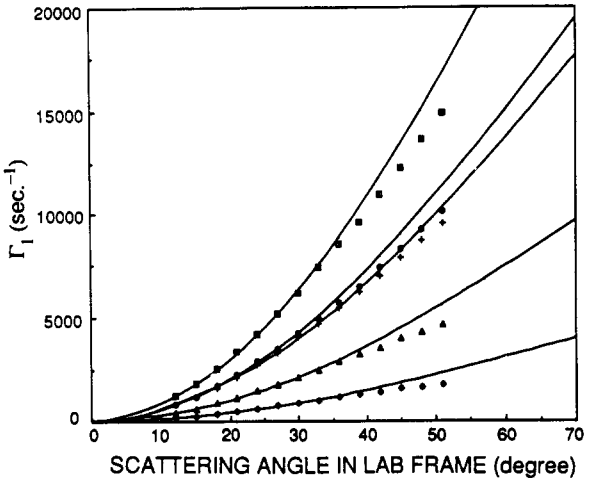

Figure 8. Experimental and calculated decay rates of dynamic light scattering from pure 5CB and LCP mixtures (M_n = 57 000) for geometry A at T = 30 °C: (—) calculated; (⊡) pure 5CB; (●) 1.5% LCP mixture; (+) 3% LCP mixture; (▲) 8% LCP mixture; (◇) 15% LCP mixture. Calculated values are for mode 1 only; deviations between experiment and calculation at higher scattering angles are due to contribution from mode 2.

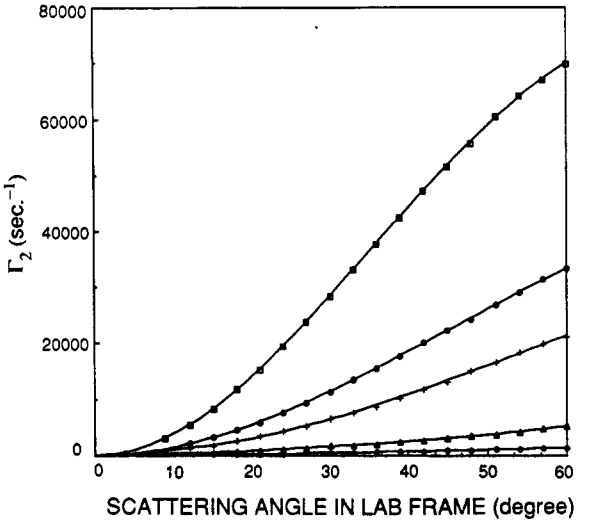

Figure 9. Experimental and calculated decay rates of dynamic light scattering from pure 5CB and the LCP mixture (M_n = 57 000) for geometry B at T = 30 °C. Symbols used here are as in Figure 8.

in the corresponding viscosity coefficient. Referring first to the decay rates, it is evident in Table I that, at T = 25.2 and 30.2 °C, the decrease in decay rate of the bend fluctuation is much larger (~−40%) in contrast to the changes in splay (~−15%) and twist (~−23%). However, at T = 33 °C, the relative decrease in decay rate is similar for all three modes.

To explore the influence of polymer concentration and molecular weight on the viscoelastic parameters, we carried out light scattering experiments in all three configurations on mixtures in 5CB of the highest molecular weight sample (MSHMA/57, M_n = 57 000), at T = 30.2 °C over a concentration range 0–15% w/w. The measured decay rates for each scattering configuration together with the calculated values based on eqs 8 and 11 are shown in Figures 8–10. The fit parameters are given in Table II. We find a pattern of behavior similar to that seen for the low molecular weight polymer (Table I), in that the addition of polymer has the largest effect on the decay rates of the bend mode and smallest on the splay mode. However, the effect is apparently more dramatic for the

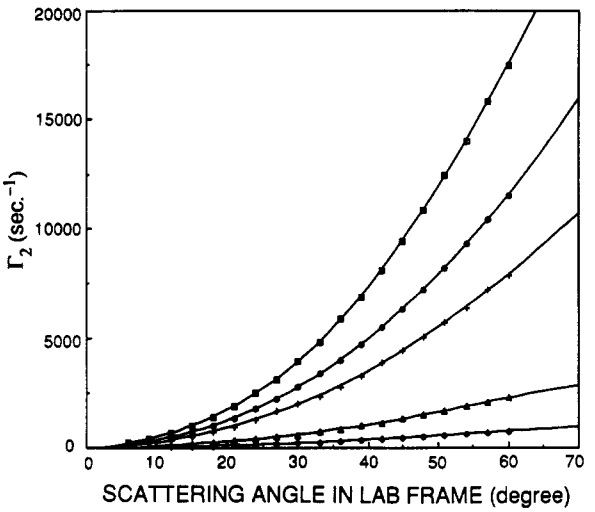

Figure 10. Experimental and calculated decay rates of dynamic light scattering from pure 5CB and LCP mixture (M_n = 57 000) for geometry C at T = 30 °C. Symbols used here are as in figure 8.

Table II
Concentration Dependence of Viscoelastic Parameters for 5CB and LCP/5CB Mixture (M_n = 57 000) at T = 30 °C

	LCP concn, w/w %				
	0	1.5	3.0	8.0	15
$10^8K_{11} \pm 5\%$, dyn	47	40	47	44	28
$10^8K_{22} \pm 3\%$, dyn	32	29	25	14	7.0
$10^8K_{33} \pm 3\%$, dyn	56	50	41	19	9.6
$K_{33}/K_{11} \pm 8\%$	1.2	1.3	0.87	0.43	0.35
$\eta_{splay} \pm 1\%$, P	0.496	0.643	0.790	1.39	2.09
$\gamma_1 \pm 1\%$, P	0.498	0.646	0.795	1.40	2.10
$\eta_{bend} \pm 2\%$, P	0.103	0.240	0.343	0.650	1.33
$10^7K_{11}/\eta_{splay} \pm 5\%$ cm^2/s	9.48	6.22	5.95	3.16	1.32
$10^7K_{22}/\gamma_1 \pm 3\%$, cm^2/s	6.32	4.44	3.14	0.979	0.333
$10^7K_{33}/\eta_{bend} \pm 3\%$, cm^2/s	54.4	20.8	11.9	2.92	0.722

higher molecular weight. Thus, in Table II, for c = 3.0% w/w, $\tilde{\Gamma}_{bend}$ decreases by 78%, $\tilde{\Gamma}_{twist}$ by 50%, and $\tilde{\Gamma}_{splay}$ by 37%, whereas, in Table I, $\tilde{\Gamma}_{bend}$ decreases by 45%, $\tilde{\Gamma}_{twist}$ 23%, and $\tilde{\Gamma}_{splay}$ by 16%. We note parenthetically that small differences in the fit parameters for pure 5CB, evident when Tables I and II are compared, may be due to differences in the cell thickness[5] used in each experiment (12.5 vs 50 μm).

It is evident, particularly for the mixture containing the high molecular weight polymer (Table II), that the major contribution to the decrease in decay rates comes from an increase in the viscosity coefficient. Again, the relative change is largest for the bend viscosity. To see this, we define the intrinsic quantity $[\eta_{bend}] = \Delta\eta_{bend}/c\eta_{bend}^0 = 80$ g/g, where $\Delta\eta_{bend} = \eta_{bend}(\text{mixture}) - \eta_{bend}^0$, c is concentration (grams per gram), and the superscript 0 refers to the pure solvent (5CB). In contrast, $[\eta_{splay}] = \Delta\eta_{splay}/c\eta_{splay}^0 \simeq [\gamma_1] = \Delta\gamma_1/c\gamma_1^0 = 21$ g/g. For the low molecular weight polymer, we obtain, at T = 30.2 °C, $[\eta_{bend}] = 16.7$ g/g and $[\eta_{splay}] \simeq [\gamma_1] = 3$ g/g. The apparent molecular weight exponent is 0.6 for $[\eta_{bend}]$ and 0.9 for $[\gamma_1]$ and $[\eta_{splay}]$. Note that the precision of these exponents is comparatively low, particularly for $[\gamma_1]$ and $[\eta_{splay}]$, because of the small viscosity increments in the low molecular weight sample.

All three elastic constants decrease on addition of polymer, but the magnitude of the change again seems largest for the bend distortion. Specifically, for the change in ΔK_{ii} with unit concentration, we observe ΔK_{11}:ΔK_{22}:ΔK_{33} = 13:16:31, indicating that the presence of polymer decreases the distortion energy in the order splay < twist < bend. A slightly different pattern of behavior was observed by Coles and Sefton[14] for mixtures of a side-chain LCP with a siloxane backbone in 5CB, viz. $\Delta K_{22} < \Delta K_{11} \ll \Delta K_{33}$.

To summarize, our light scattering results indicate that the dissolution of a side-chain LCP in a low molar mass nematic decreases the relaxation rates of director distortions in the order $|\Delta\tilde{\Gamma}_{bend}| \gg |\Delta\tilde{\Gamma}_{twist}| > |\Delta\tilde{\Gamma}_{splay}|$. Increase of polymer molecular weight magnifies the decrease in decay rates. The effect arises because of a combination of a moderate decrease in the elastic constants and a large increase in the viscosity coefficients. The Freedericksz transition measurements suggest that the decrease in elastic constants at a fixed temperature may be largely due to the decrease in order parameter which accompanies a lowering of the nematic–isotropic transition temperature on addition of polymer. Our observations that $[\eta_{bend}] \gg [\gamma_1] \sim [\eta_{splay}]$ are consistent with the interpretation that the presence of the side-chain LCP substantially restricts the amplitude of the bend distortion. This arises presumably because the mesogen is at least partially coupled to the backbone, and the bend displacement requires motions normal to the backbone, in contrast to the twist and splay distortions, which involve relatively unhindered motions around the backbone.

Acknowledgment. We are grateful to Dr. K. Devanand, Akhtar Saeed, and Gregory DiLisi for assistance with sample preparation and light scattering analysis during the initial stages of this work. Finally, we thank the National Science Foundation for support through DMR MRG 01845.

References and Notes

(1) DeGennes, P.-G. *The Physics of Liquid Crystals*; Oxford University Press: Oxford, U.K., 1974, Chapters 3 and 5.
(2) de Jen, W. H. *Physical Properties of Liquid Crystalline Materials*; Gordon & Breach: New York, 1980; Chapters 6 and 7.
(3) Orsay Liquid Crystal Group. *J. Chem. Phys.* **1969**, *51*, 816.
(4) Orsay Liquid Crystal Group. *Phys. Rev. Lett.* **1969**, *22*, 1361.
(5) Sefton, M. S.; Bowdler, A. R.; Coles, H. J. *Mol. Cryst. Liq. Cryst.* **1985**, *129*, 1.
(6) Da, X.; Paul, G. L. *Mol. Cryst. Liq. Cryst.* **1987**, *1506*, 177.
(7) Leslie, F. M. *Q. J. Mech. Appl. Math.* **1966**, *19*, 357.
(8) Miesowicz, M. *Bull. Int. Acad. Pol. Sci. Lett. Ser. A* **1936**, *28*, 228.
(9) Max, B.; Wolf, E. *Principles of Optics*; Oxford University Press: Oxford, U.K., 1980; Chapter 14.
(10) See ref 1, p 85; also ref 2, p 76.
(11) Taratuta, V.; Hurd, A. J.; Meyer, R. B. *Phys. Rev. Lett.* **1985**, *55*, 246. Se, K.; Berry, G. C. *Mol. Cryst. Liq. Cryst.* **1987**, *153*, 133.
(12) Casagrande, C.; Fabre, P.; Veyssie, M.; Weill, C.; Finkelmann, H. *Mol. Cryst. Liq. Cryst.* **1984**, *113*, 193.
(13) Hopwood, A. J.; Coles, H. J. *Mol. Cryst. Liq. Cryst.* **1985**, *130*, 281.
(14) Coles, H. J.; Sefton, M. S. *Mol. Cryst. Liq. Cryst. Lett.* **1985**, *1* (5), 159.
(15) Percec, V.; Tomazos, D. *J. Polym. Sci. Part A, Polym. Chem.* **1989**, *27*, 999. Percec, V.; Tomazos, D.; Pugh, C. *Macromolecules* **1989**, *22*, 3259.
(16) Karat, P. P.; Madhusudana, N. V. *Mol. Cryst. Liq. Cryst.* **1976**, *36*, 51.
(17) Vaz, N. A.; Smith, G. W.; Montgomery, G. P.; Marion, W. D.; Percec, V.; Lee, M. *Mol. Cryst. Liq. Cryst.* in press.
(18) Bradshaw, M. J.; Ranes, E. P. *J. Phys.* **1985**, *46*, 1513.
(19) Skarp, K.; Lagerwall, S. T.; Stebler, B. *Mol. Cryst. Liq. Cryst.* **1980**, *60*, 215.
(20) Hara, M.; Hirakata, J. I.; Togoota, T.; Takezoe, H.; Fukuda, A. *Mol. Cryst. Liq. Cryst.* **1985**, *122*, 161.
(21) Madhusudana, N. V.; Pratibha, R. *Mol. Cryst. Liq. Cryst.* **1982**, *89*, 249.

Registry No. 5CB, 40817-08-1; MSHMA, 120416-97-9.